Lawrence Berkeley National Laboratory

Title

Determination of ionization energies of CnN (n=4-12): Vacuum-ultraviolet (VUV) photoionization experiments and theoretical calculations

Permalink

https://escholarship.org/uc/item/7z3312nx

Author

Kostko, Oleg

Publication Date

2010-10-05

Determination of ionization energies of C_nN (n=4-12): Vacuum-ultraviolet (VUV) photoionization experiments and theoretical calculations

Oleg Kostko,[1] Jia Zhou,[1] Bian Jian Sun,[2] Jie Shiuan Lie,[2] Agnes H.H. Chang,[2] Ralf I. Kaiser,[3] and Musahid Ahmed[1]*

[1]*Chemical Sciences Division, Lawrence Berkeley National Laboratory, Berkeley, CA 94720.*

[2]*Department of Chemistry, National Dong Hwa University, Hualien, Taiwan.*

[3]*Department of Chemistry, University of Hawaii at Manoa, Honolulu, HI 96822.*

* Corresponding author: MAhmed@lbl.gov

Abstract

Results from single photon vacuum ultraviolet photoionization of astrophysically relevant C_nN clusters, n

= 4 - 12, in the photon energy range of 8.0 eV to 12.8 eV are presented. The experimental

photoionization efficiency curves, combined with electronic structure calculations, provide improved

ionization energies of the C_nN species. A search through numerous nitrogen-terminated C_nN isomers for

n=4-9 indicates that the linear isomer has the lowest energy, and therefore should be the most

abundant isomer in the molecular beam. Comparison with calculated results also shed light on the

energetics of the linear C_nN clusters, particularly in the trends of the even-carbon and the odd-carbon

series. These results can help guide the search of potential astronomical observations of these neutral

molecules together with their cations in highly ionized regions or regions with a high UV/VUV photon

flux (ranging from the visible to VUV with flux maxima in the Lyman-α region) in the interstellar

medium.

Keywords: Laser ablation, molecular beams, synchrotron radiation, electronic structure theory

1. Introduction

During the last decades, the spectroscopic (Grutter et al. 1999) and thermodynamic properties (Belbruno et al. 2001; Golovin & Takhistov 2004) of nitrogen-terminated carbon clusters of the generic formula C_nN have received considerable attention due to their role in the astrochemical evolution of the interstellar medium (Fuchs et al. 2004; Hasegawa & Herbst 1993; Herbst & Leung 1989) and their contribution to the cosmic carbon budget (Agundez et al. 2008; Eichelberger et al. 2007; Redman et al. 2003; Ziurys 2006). These radicals are linear in nature, belong to the $C_{\infty v}$ point group, and are considered as building blocks to form hydrogen-deficient polycyclic aromatic hydrocarbon molecules (PAHs) and possibly carbonaceous grain particles in the outflow of carbon stars.

Considering the odd-carbon nitrogen-terminated clusters, the low molecular weight species CN, C_3N, and C_5N hold $^2\Sigma^+$ electronic ground states with the $^2\Pi$ states being higher in energy by 9242, 1844, and 455 cm^{-1}, respectively (Botschwina 2003; Herzberg & Phillips 1948; Hoshina & Endo 2007). Higher members hold a $^2\Pi$ electronic ground state (Zhang et al. 2003). The simplest representative of this series, the cyano radical $CN(X^2\Sigma^+)$, was discovered by McKellar (1940) and subsequently confirmed by Adams (1941) toward the bright star ζ Ophiuchi. The next higher member, the $C_3N(X^2\Sigma^+)$ radical, was observed toward the dying carbon star IRC+10216 via the doublets of the J = 10 $\rightarrow$ 9 and J = 9 $\rightarrow$ 8 transitions (Guelin & Thaddeus 1977); Friberg et al. (1980) also monitored the N = 3 $\rightarrow$ 2 hyperfine structure at 29.7 GHz toward the cold molecular clouds TMC-1 and TMC-2. It took almost three decades before the cyanobutadienyl radical, $C_5N(X^2\Sigma^+)$, was observed in TMC-1 and also tentatively toward the circumstellar envelope of IRC+10216 (Guelin et al. 1998). This radical species was found to have fractional abundances two orders of magnitude less than the related closed shell cyanodiacetylene molecule (HC_5N). It should be noted that very recently, two negative anions, C_3N^- and C_5N^-, (Cernicharo

3

et al. 2008; Thaddeus et al. 2008) were detected in the circumstellar envelope of IRC+10216. A quantitative analysis suggested that the column density of C_3N^- is about 0.5% that of C_3N.

Considering the fact that only odd-carbon members (CN, C_3N, C_5N) have been detected so far, astronomers and physical chemists suggested plausible formation pathways involving photodissociation and neutral-neutral reactions (Doty & Leung 1998; Stauber et al. 2004). Photodissociation of the closed shell $HC_{2n+1}N$ precursors such as the ubiquitous interstellar hydrogen cyanide (HCN), cyanoacetylene (HC_3N), and cyanodiacetylene (HC_5N) presents an elegant, one-step route for the formation of hitherto detected $C_{2n+1}N$ members (Figure 1). Bimolecular neutral reactions, such as the reaction of ground state dicarbon molecules, $C_2(X^1\Sigma_g^+)$, with hydrogen cyanide (HCN), were found to represent exoergic reaction pathways without an entrance barrier, which can lead, for instance, to the formation of linear cyanoethynyl $C_3N(X^2\Sigma^+)$ radical (Gu et al. 2009). Similarly, a reaction of singlet dicarbon with cyano-acetylene molecule (HC_3N) should yield the cyanobutadienyl radical, $C_5N(X^2\Sigma^+)$. These reaction schemes are also expected to lead to higher, hitherto unobserved, odd-carbon species like $C_7N(X^2\Sigma^+)$ and $C_9N(X^2\Sigma^+)$. Lastly, Maclean et al. (2007) suggested a more exotic route of formation via charge stripping of the corresponding anions in the gas phase.

The failed detection of the even-carbon clusters could be attributed to various factors. Production mechanisms could be unfavorable. For instance, the reaction of ground state carbon atoms with hydrogen cyanide yielding $C_2N(X^2\Pi)$ plus atomic hydrogen was found to be strongly endoergic and, hence, suggested to be unlikely in cold molecular clouds (Mebel & Kaiser 2002). On the other hand, electronic structure calculations proposed that the exoergic and entrance-barrier less reaction of ground state atomic carbon with the next higher member, cyanoacetylenes (HC_3N), yields exclusively the linear $C_4N(X^2\Pi)$ radical plus atomic hydrogen (Li et al. 2006). Alternatively, the radicals could be easily photolyzed or ionized in less shielded regions of the interstellar medium such as close to the carbon star

IRC+10216 or in the outer regions of cold molecular clouds. Furthermore, the small dipole moment of the $^2\Pi$ ground state of the even-carbon species and the larger odd-carbon species compounds the difficulty in their detection via microwave spectroscopy (Botschwina 2003; McCarthy et al. 2003).

Therefore, to guide the search for hitherto undetected C_nN clusters and possible their singly ionized counterparts, it is important to provide data on their ionization energies (IEs). These IEs can be utilized not only to judge to what extent neutral clusters can be ionized in harsh, poorly shielded radiation environments of the interstellar medium, but they can also be incorporated into thermodynamic cycles to extract the enthalpies of formation of nitrogen-terminated carbon clusters. These energies, in turn, can be included into novel astrochemical models to constrain the column densities of hitherto unobserved C_nN clusters. However, accurate data on IEs of C_nN clusters are surprisingly scarce. A detailed literature research indicated that the 'best' IEs have significant errors. Even the simplest member, the cyano radical, holds cited IEs between 14.0 and 14.5 eV (Berkowitz 1962; Dibeler et al. 1961). The IEs for C_2N, C_3N, and C_4N have been reported to be 12-13 eV (Dibeler, et al. 1961; Lias et al. 1988), about 14.3 eV (Dibeler, et al. 1961), and 12.3 eV (Dibeler, et al. 1961), respectively. The main uncertainties originate from the poorly defined energy spread of the electron beam utilized to ionize the neutral precursor molecules via electron impact ionization and assumption about the precursors and formation of the C_nN species. Most importantly, experimental IEs of clusters higher than n = 6 are completely absent.

Here, we present a combined experimental and theoretical study on the adiabatic ionization energies (AIEs) of C_nN clusters. The AIE presents one of the most relevant thermochemical measure-ments: ionization energies can be utilized to determine the nature of the structural isomers, as well as be combined with thermochemical cycles to obtain enthalpies of formation (Kaiser et al. 2007). By producing the nitrogen-carbon clusters *in situ* in a supersonic beam and utilizing tunable vacuum

ultraviolet (VUV) radiation from the Advanced Light Source to photoionize the neutral clusters, we provide *recommended* IEs of C_nN clusters up to $C_{12}N$ based on a comparison of the ionization onsets observed in the photoionization efficiency (PIE) curves with the theoretical AIEs. We will also present an analysis on the structures of these clusters, i.e. linear versus cyclic, and discuss the inherent energetics and stabilities. We hope that these experimental and theoretical data can be exploited to plan future astronomical searches for hitherto unobserved C_nN molecules in the interstellar medium.

2. Experiment

The experiments are performed on a laser ablation apparatus coupled to a 3 m monochromator at the Chemical Dynamics Beamline (9.0.2) at the Advanced Light Source. The experimental apparatus used for the cluster production is the same as used recently for preparation of gas phase SiO_2 (Kostko et al. 2009) and carbon clusters (Nicolas et al. 2006). It consists of a laser ablation molecular beam cluster source and a reflectron time-of-flight (TOF) mass spectrometer. A rotating and translating 6.35 mm diameter graphite rod inside a Smalley-type cluster source is ablated by focused radiation from the second harmonic (532 nm) of a 50 Hz pulsed Nd:YAG laser. The ablation laser energy employed in this study is ~0.62 mJ/pulse. A beam of pure nitrous oxide (N_2O; supplier Matheson Tri-Gas, 99.995% purity) is introduced through a pulsed valve located behind the rod for the cooling of the ablated material; backing pressure of nitrous oxide is ~240 kPa. The N_2O gas reacts with ablated carbon clusters and give rise to a series of C_nN and C_nO clusters. The temperature of the clusters after travelling through a 25 mm long, 4 mm diameter, room temperature nozzle is estimated to be about 300 K. It was observed that the PIE curve of tricarbon (C_3) obtained using the same setup shows a sharper onset than was observed previously, demonstrating efficient cooling and quenching of electronically and vibrationally excited states in this work. Ionized clusters produced directly in the ablation region are deflected out of the molecular beam by a ~700 V cm^{-1} electrical field. The neutral cluster beam is skimmed and ionized

by synchrotron VUV radiation inside the interaction region of a reflectron TOF mass spectrometer. Since the synchrotron light is quasi-continuous (500 MHz), a pulsed field directing the photoionized clusters into the flight tube is used as a start pulse for the TOF measurement. This pulse is synchronized with the ablation laser and pulsed valve. After acceleration and passage through the flight tubes and reflectron, ions are detected by a microchannel plate detector. The time-dependent signal is amplified by a fast preamplifier, collected by a multichannel-scalar card and analyzed with a PC computer. Each mass spectrum was recorded for 2000-5000 sweeps at a repetition rate of 50 Hz. The PIE curves are obtained by integrating over the peaks in the mass spectrum at each photon energy. The synchrotron VUV photon flux used for spectra normalization is measured by a silicon photodiode. Argon or krypton gases (for the low photon energy region) are used in a gas filter to block the higher harmonics of the undulator synchrotron radiation. Absorption lines of argon are used for energy calibration of the PIE spectra.

3. Results

The mass spectrum recorded at a fixed photon energy of 12.5 eV is shown in Figure 2a. A progression of clusters comprising the series C_n, C_nN and C_nO is observed up to mass–to-charge, m/z, of 200. The most prominent peak in the mass spectrum is C_3^+; this is similar to what has been previously observed in the VUV photoionization of pure carbon clusters (Belau et al. 2007). Figure 2b shows the peak intensities for C_nN^+ clusters at photon energies of 11.5 eV and 12.5 eV. It is apparent that at both photon energies the even-carbon clusters (i.e. $C_{2n}N$) are more prominent than the odd-carbon clusters (i.e. $C_{2n+1}N$) for the smaller cluster sizes. However, for the larger clusters, there is no such clear pattern.

Signals for C_nN (n = 3 - 12) were strong enough to allow measurements of PIE curves. A photon energy scan in 0.1 eV steps from 8.5 to 12.8 eV is shown in Figure 3 for n = 3 - 10. The PIE curves have been normalized to allow for comparison of various sized clusters. The most striking feature in Figure 3 is the difference between the PIE curve of C_3N and those of C_4N and C_5N. While the experimental IE for

C_3N is difficult to ascertain due to possible contributions from dissociation of larger clusters below 12.5 eV, it is still apparent that the photoionization cross section shows a significant shift toward lower energy for n > 3. For the larger clusters, such a dramatic change in the ionization onset is not observed. Also notable is that above 11.5 eV, the PIE curves of C_nN (n = 4 - 10) are similarly shaped, while between 9.5-11.0 eV, there is enhancement in signal for n $\geq$ 7.

To ascertain the trends and generate reliable ionization onsets, a series of PIE curves for n = 4 - 12 were recorded, in finer steps of 0.05 eV between 8.0 and 11.4 eV. The results are shown for an average of 7 datasets in Figures 4 and 5 for the even-carbon and the odd-carbon clusters, respectively. Both series show decreasing ionization onsets with increasing cluster size. For the even-carbon series, the ionization onset decreases from 9.6 ± 0.1 eV for C_4N to 8.4 ± 0.2 eV for $C_{12}N$. Also present in the PIE curves of the even-carbon species is a second, more gradual onset at about 1.3 eV after the first sharp onset.   This becomes particularly noticeable starting with C_6N. The odd-carbon series have higher ionization onsets than the even-carbon series, with C_5N having an onset at 10.4 ± 0.1 eV and gradually decreasing to 8.7 ± 0.2 eV for $C_{11}N$. Although C_7N has a very sharp second onset at 10.55 eV, the other species of the odd-carbon series only have a gradual initial onset that resembles the second onset of the even-carbon series. The error in the experimental measurements are shown with grey shading in Figures 4 and 5, and while it would appear that the signal-to-noise is not very good given the 50 Hz repetition rate of the experiment, it does show onsets and changes in shapes quite clearly.

4. Electronic Structure Calculations

In order to assist the interpretation of these PIE curves, electronic structure calculations were carried out to determine the AIEs of the linear and probable ring-containing isomers for each C_nN molecule. The optimized geometries and harmonic frequencies of neutral and cationic C_nN species are obtained at the level of hybrid density functional theory (DFT), B3LYP/cc-pVTZ.   The single point

CCSD(T)/cc-pVTZ energies with B3LYP/cc-pVTZ zero-point energy corrections are computed for n = 1-11, unless stated otherwise. DFT is known to perform poorly in obtaining the energies. Specifically, it underestimates the barriers of chemical reactions, the band gaps of materials, the energies of dissociating molecular ions, and charge transfer energies (Cohen et al. 2008). On the other hand, DFT optimized geometries show good agreement with MP2, CCSD(T), and experimental results for the related systems of cumulene and polyyne isomers (C_3H_4, C_5H_4, and C_7H_4) (Woodcock et al. 2002), and likewise, for C_nN clusters, match well with experiment (Belbruno, et al. 2001; Chuchev & BelBruno 2002). Thus the combination of B3LYP/cc-pVTZ optimized geometries and CCSD(T)/cc-pVTZ energies for the present calculations of 218 C_nN (n=1-14) species is valid in terms of chemical accuracy and computer efficiency. Among these 218 species, 15 linear and 12 cyclic species have been investigated in previous theoretical works (Belbruno, et al. 2001; Botschwina 1996; Botschwina et al. 1997; Chuchev, et al. 2002; Ding et al. 2001; Green 1980; Maclean, et al. 2007; Mebel, et al. 2002; Pauzat et al. 1991; Resat et al. 1994; Wang et al. 2009) in which the geometries were obtained almost exclusively by DFT since 2001, with an exception of the relatively small C_3N^+ computed by CASSCF. Furthermore, C_4H_2 and C_6H_2 are used as test cases where the calculated IEs, 10.06 eV and 9.42 eV, respectively, are in good agreement with the experimental values of 10.17 eV and 9.50 eV, respectively (Bieri et al. 1977).

For the analysis of the present C_nN PIE curves, the AIEs of each isomer is calculated by taking the energy difference, with zero-point energy corrections, between the respective cationic and neutral counterparts. Because the neutral isomers have a doublet ground state, the removal of an electron can form a singlet cation or a triplet cation, leading to two calculated AIEs for each isomer. GAUSSIAN98 (Frisch et al. 2001) and GAUSSIAN03 (Frisch et al. 2004) programs are employed in the calculations. Figure 6 shows the optimized geometries of the neutral C_8N isomers, where the relative energies are indicated and the nomenclature for various isomers can be gleamed. As is the case with C_8N, the theoretical results indicate that for all the C_nN clusters studied here, the linear geometry is the lowest

9

energy isomer for the neutral molecules. However, several ring-containing isomers, such as the $[C_3]C_{n-3}N$ isomers of the even-carbon series, are less than 0.35 eV above the linear isomer. The calculated AIEs, to the cation singlet and triplet manifold, of the three lowest energy isomers for each cluster size are shown in Figures 4 and 5 along with the experimental PIE curves; for n=10-12, only the linear and cyclic isomer AIEs are shown. The experimental and calculated values associated with Figures 4 and 5 are listed in Table 1. Detailed calculation results, including geometries, vibrational frequencies, and rotational constants are included in the supplementary information.

5. Discussions

The electronic structure calculations of the C_nN molecules point to the linear isomer as the most abundant isomer in the molecular beam. The linear C_nN radicals exhibit two classes of chemical structures—the molecules containing odd number of carbons have more polyacetylenic bonding structure with alternating single and triple bonds, and the molecules containing even number of carbons tend toward more cumulenic bonding structure. These differences are more pronounced for smaller clusters and in part account for the oscillatory intensities observed in Figure 2b. Due to this difference in chemical structure, the odd-carbon and even-carbon linear isomers are expected to exhibit different trends and behaviors, and they are discussed separately in the following sections.

For the even-carbon clusters, the experimental PIE curves show an initial onset that is ~0.2 eV higher than the calculated AIEs to the singlet state of the linear cation; this onset has a sharp appearance as seen in Figure 4. Shown in Figure 7 are the optimized geometries of the linear isomers for C_nN (n=4-13) including the neutral doublet ground state and the cation singlet and triplet states. Comparing the geometries of the neutral molecule to the cation singlet state for the even-carbon species, one can see that there is not a significant change in geometry upon ionization to the singlet state. Therefore, the PIE curves should exhibit a sharp onset in accordance with the Franck-Condon

10

principle. On the other hand, ionization to the cation triplet state would result in a large change in geometry, causing the onset for the triplet state to be more gradual. This is indeed the case for the second onset in the PIE curves of the even-carbon species. Furthermore the calculated AIEs to the cation triplet state are in the same energy range. For this reason, we tentatively assign the second onset in the PIE curves of C_6N, C_8N, $C_{10}N$, and $C_{12}N$ to be the IEs to the cation triplet state of the linear isomer, resulting in the experimental values of 10.3 ± 0.1 eV, 9.9 ± 0.2 eV, 9.9 ± 0.2 eV, and 9.6 ± 0.3 eV, respectively. It is of interest to note that the cation singlet state appear to have a smaller photoionization cross section than the cation triplet state, as the signal intensity rises several folds after the onset of the triplet state.

The linear isomers of the odd-carbon species have much smaller calculated singlet-triplet splittings, and in all cases, the calculated AIEs to the cation triplet state are lower than the singlet state. Figure 7 shows that for the odd-carbon clusters there is a significant change in geometry upon ionization to both the cation singlet state and the triplet state, which would result in a slow onset as observed in the experimental PIE curves shown in Figure 5. In fact, the initial onset of the odd-carbon species appears similar to the triplet onset of the even-carbon species, which also has a large change in geometry as discussed above. Given that the cation singlet state has a smaller photoionization cross section than the triplet state, the experimentally observed onsets of the odd-carbon clusters likely correspond to the IEs to the cation triplet state. The onset of the cation singlet state is in all likelihood buried within the triplet onset. Of all the odd-carbon clusters studied here, only C_7N exhibits an obvious second onset, at 10.55 eV, which is very sharp unlike the ones observed for even-carbon species. Although the calculated AIE to the cation triplet state of the $[C_6]CN$ isomer lies nearby at 10.3 eV, the fact that no experimental onset is observed for the cation singlet state of that low-lying isomer makes it unlikely that the sharp second onset is due to isomer contribution. The only other likely explanation is

11

an excited electronic state on the cation surface, and given the sharpness of the onset, this excited electronic state has a geometry very similar to the neutral molecule.

Shown in Figure 8 are the experimentally observed ionization onsets compared with the calculated AIEs to the cation singlet and triplet states of the linear isomers. The oscillatory nature of the graphs are due to the difference between the even-carbon and odd-carbon series as discussed above. One can see that both the CCSD(T) and B3LYP energies agree fairly well with experimental values up to n = 9. However, the larger clusters, n ≥ 10, show some significant deviation between experimental values and calculated AIEs, particularly for the even-carbon species. One possible reason for this discrepancy could be the presence of multiple isomers in the molecular beam. As Figure 2b shows, at the cluster sizes where the differences between theory and experiment increase, there is a change to the intensity pattern of the C_nN^+ clusters in the mass spectrum. With clusters of n < 10, the even-carbon species are more intense than the odd-carbon species, whereas for the larger clusters, there is no such clear and distinct trend. This change in mass spectral intensity can very well be caused by increased presence of different isomers for the larger C_nN clusters.

At this point, we should discuss further the isomeric population in the molecular beam. Due to the method of production of the C_nN clusters, i.e. via ablation of pure carbon rod with N_2O backing gas, the theoretical search for isomers were performed only for nitrogen-terminated C_nN species, as these clusters are the most likely to form under the experimental conditions. Furthermore, previous calculations have shown that in the case of C_6N, the C_nNC_n isomers are at least 1 eV above the linear isomer (Chuchev, et al. 2002), making their formation in the molecular beam unfavorable. For the smaller odd-carbon clusters, it is not likely that non-linear isomers contribute to the observed PIE curves, as they are calculated to lie significantly higher in energy than the linear isomer. For even-carbon species, the $[C_3]C_{n-3}N$ partially cyclic isomer lies within 0.35 eV of the linear isomer; in the case of

12

C_4N, the $[C_3]CN$ isomer is only 0.08 eV above. Energetically, it is certainly possible for this isomer to exist in the molecular beam. The presence of the $[C_3]CN$ isomer could explain why the PIE curve of C_4N does not exhibit a clear second onset like the other even-carbon species. Unfortunately, this also means that it is not possible to determine an experimental IE for the $[C_3]CN$ isomer. For C_6N and C_8N, it is difficult to say whether there is a significant contribution from another isomer based on the PIE curves, particularly for the case of C_8N, where all the calculated AIEs for the lowest-lying isomers lie within 0.2 eV of each other.   For most C_nN species, however, the calculated results for the linear isomer are adequate in explaining the experimentally observed PIE curves, and therefore lead us to believe that the linear isomer dominates the population in the molecular beam. Unfortunately, for the larger C_nN clusters, n ≥ 10, an extensive search for isomers were not possible due to computational cost, and therefore we cannot ascertain the presence of other isomers in the molecular beam, especially given that the experimental IEs do not agree well with the calculated AIEs of the linear isomer. Furthermore, the general trend in the isomeric energetics points to more low-lying isomers with increasing cluster size, making it likely for the larger C_nN clusters to have a mixed isomeric population in the molecular beam. Of interest is also the presence of the completely cyclic isomer. However, the calculations indicate that the cyclic isomer lies more than 2 eV above the linear isomer for n = 3 - 8. Even for $C_{12}N$, the largest cluster studied here, the cyclic isomer is still 0.84 eV above the linear isomer. The cyclic isomers are also calculated to have significantly lower IEs than the linear isomer. Given these energetics, it is unlikely that the cyclic isomer is a significant presence in the molecular beam.

6. **Astrophysical Implications**

Single photon ionization of C_nN clusters, n = 4 - 12, in the photon energy range of 8.0-12.8 eV is presented. The experimental PIE curves, combined with theoretical ionization energy calculations, provide improved IEs of the C_nN species. Distinctive trends are observed for the even-carbon and odd-

carbon series. In particular, a gradual decrease in ionization onset as cluster size increases is observed for both series. A search for nitrogen-terminated C_nN isomers for n=4-9 indicate that the linear isomer has the lowest energy, and therefore should be the most abundant isomer in the molecular beam. Comparison with calculated results also indicates that the ionization to the cation singlet and triplet manifold of the linear even-carbon isomer is observed experimentally, while for the odd-carbon species only the triplet ionization onset is observed. The experimental PIE curves agree with the theoretical results that there are large geometry changes upon ionization for the odd-carbon linear isomers, while ionization to the cation singlet state of the even-carbon linear isomers show little geometry change.

In previous studies, Dibeler et al.(1961) reported the appearance energies of C_3N, C_4N, C_5N and C_6N to be 14.3, 12.3, 12.0 and 12.2 eV, respectively, following electron impact ionization of a series of homologues of dicyano acetylenes. It is apparent that in all cases, these values are not correct when compared to the results presented in this work. The authors made an assumption that the observed cations arose not only from dissociative photoionization of neutral species, but that species of the form C_nN was present in the molecular beam through the pyrolytic decomposition of the parent molecule. It would appear, however, that this assumption was incorrect. The new experimental ionization energies for the C_nN (n = 4 - 12) clusters presented in Table 1 should therefore provide more accurate values in future astrochemical models. Recall that the molecular nature of interstellar environments such as cold molecular clouds, diffuse clouds, or planetary nebulae provide a clock to probe the physical conditions such as temperature and the radiation field. The UV/VUV (ranging from the visible to VUV with flux maxima in the Lyman-α region) field close to central stars, such as in the vicinity of planetary nebulae, has the capability not only to photodissociate, but also to photoionize molecules (Tenenbaum et al. 2009). Therefore, the 'inventory' of neutral circumstellar molecules and radicals can be greatly influenced by intense UV/VUV photoionization processes, yielding, for instance, singly ionized, nitrogen-

14

terminated carbon clusters as observed in the present experiments. We hope that the present work will guide future astronomical observations of this class of molecular cations in the interstellar medium.

References

Adams, W. S. 1941, ApJ, 93, 11

Agundez, M., Fonfria, J. P., Cernicharo, J., Pardo, J. R., & Guelin, M. 2008, A&A, 479, 493

Belau, L., et al. 2007, J. Am. Chem. Soc., 129, 10229

Belbruno, J. J., Tang, Z. C., Smith, R., & Hobday, S. 2001, Mol. Phys., 99, 957

Berkowitz, J. 1962, J. Chem. Phys., 36, 2533

Bieri, G., Burger, F., Heilbronner, E., & Maier, J. P. 1977, Helv. Chim. Acta, 60, 2213

Botschwina, P. 1996, Chem. Phys. Lett., 259, 627

Botschwina, P. 2003, Phys. Chem. Chem. Phys., 5, 3337

Botschwina, P., Horn, M., Markey, K., & Oswald, R. 1997, Mol. Phys., 92, 381

Cernicharo, J., Guelin, M., Agundez, M., McCarthy, M. C., & Thaddeus, P. 2008, ApJL, 688, L83

Chuchev, K., & BelBruno, J. J. 2002, J. Phys. Chem. A, 106, 4240

Cohen, A. J., Mori-Sanchez, P., & Yang, W. T. 2008, Science, 321, 792

Dibeler, V. H., Reese, R. M., & Franklin, J. L. 1961, J. Am. Chem. Soc., 83, 1813

Ding, Y. H., Liu, J. L., Huang, X. R., Li, Z. S., & Sun, C. C. 2001, J. Chem. Phys., 114, 5170

Doty, S. D., & Leung, C. M. 1998, ApJ, 502, 898

Eichelberger, B., Snow, T. P., Barckholtz, C., & Bierbaum, V. M. 2007, ApJ, 667, 1283

Friberg, P., Hjalmarson, A., Irvine, W. M., & Guelin, M. 1980, ApJ, 241, L99

Frisch, M. J., et al. 2004, GAUSSIAN 03 (Wallingford CT: Gaussian, Inc.)

Frisch, M. J., et al. 2001, GAUSSIAN 98 (Pittsburgh PA: Gaussian, Inc.)

Fuchs, G. W., et al. 2004, Spectroscopy of Linear Carbon Chain Radicals - the Case of CnN Chains, Springer Proceedings in Physics 91, "The Dense Interstellar Medium in Galaxies" (Springer)

Golovin, A. V., & Takhistov, V. V. 2004, J. Mol. Struct., 701, 57

Green, S. 1980, ApJ, 240, 962

Grutter, M., Wyss, M., & Maier, J. P. 1999, J. Chem. Phys., 110, 1492

Gu, X., et al. 2009, ApJ, 701, 1797

Guelin, M., Neininger, N., & Cernicharo, J. 1998, A&A, 335, L1

Guelin, M., & Thaddeus, P. 1977, ApJ, 212, L81

Hasegawa, T. I., & Herbst, E. 1993, MNRAS, 263, 589

Herbst, E., & Leung, C. M. 1989, ApJS, 69, 271

Herzberg, G., & Phillips, J. G. 1948, ApJ, 108, 163

Hoshina, K., & Endo, Y. 2007, J. Chem. Phys., 127

Kaiser, R. I., Belau, L., Leone, S. R., Ahmed, M., Wang, Y. M., Braams, B. J., & Bowman, J. M. 2007, Chem. Phys. Chem, 8, 1236

Kostko, O., Ahmed, M., & Metz, R. B. 2009, J. Phys. Chem. A, 113, 1225

Li, H. Y., et al. 2006, J. Chem. Phys., 124

Lias, S. G., Bartmess, J. E., Liebman, J. F., Holmes, J. L., Levin, R. D., & Mallard, W. G. 1988, J. Phys. Chem. Ref. Data, 17, 1

Maclean, M. J., Fitzgerald, M., & Bowie, J. H. 2007, J. Phys. Chem. A, 111, 12932

McCarthy, M. C., Fuchs, G. W., Kucera, J., Winnewisser, G., & Thaddeus, P. 2003, J. Chem. Phys., 118, 3549

McKellar, A. 1940, PASP, 52, 187

Mebel, A. M., & Kaiser, R. I. 2002, ApJ, 564, 787

Nicolas, C., Shu, J. N., Peterka, D. S., Hochlaf, M., Poisson, L., Leone, S. R., & Ahmed, M. 2006, J. Am. Chem. Soc., 128, 220

Pauzat, F., Ellinger, Y., & McLean, A. D. 1991, ApJ, 369, L13

Redman, M. P., Viti, S., Cau, P., & Williams, D. A. 2003, MNRAS, 345, 1291

Resat, M. S., Smolanoff, J. N., Goldman, I. B., & Anderson, S. L. 1994, J. Chem. Phys., 100, 8784

Stauber, P., Doty, S. D., van Dishoeck, E. F., Jorgensen, J. K., & Benz, A. O. 2004, A&A, 425, 577

Tenenbaum, E. D., Milam, S. N., Woolf, N. J., & Ziurys, L. M. 2009, ApJL, 704, L108

Thaddeus, P., et al. 2008, ApJ, 677, 1132

Wang, T. F., Buntine, M. A., & Bowie, J. H. 2009, J. Phys. Chem. A, 113, 12952

Woodcock, H. L., Schaefer, H. F., & Schreiner, P. R. 2002, J. Phys. Chem. A, 106, 11923

Zhang, C. J., Cao, Z. X., & Zhang, Q. E. 2003, Chem. Res. Chinese U., 19, 454

Ziurys, L. M. 2006, P. Natl. Acad. Sci. USA, 103, 12274

Table 1: Relative energies of the neutral isomers and their respective calculated and experimental IEs.[a]

C_nN[b]	Neutral ΔE		Exp. IEs		B3LYP AIEs		CCSD(T) AIEs	
	B3LYP	CCSD(T)	Singlet[c]	Triplet[c]	Singlet[c]	Triplet[c]	Singlet[c]	Triplet[c]
l-C_4N	0	0	9.6 ± 0.1	-	9.78	11.09	9.37	10.99
[C_3]CN	0.36	0.08			10.44	10.72	10.24	10.54
[C_2N]C_2	1.67	1.58			-	10.68	-	10.50
l-C_5N	0	0	-	10.4 ± 0.1	10.53	9.73[d]	10.51	10.39[e]
C[C_3]CN	1.45	1.35			10.64	10.48	10.34	10.48
[C_2N]C_3	1.69	1.92			10.14	10.21	9.76	10.14
l-C_6N	0	0	8.95 ± 0.05	10.3 ± 0.1	9.06	10.33	8.76	10.36
[C_3]C_3N	0.59	0.34			-	10.10	-	9.97
C_2[C_3]CN	1.50	1.30			-	10.93	-	10.81
l-C_7N	-	0	-	9.8 ± 0.1	-	-	9.72	9.49
[C_6]CN	-	0.52			9.53	10.29	9.14	10.30
[C_4]C_3N	-	0.94			9.36	9.70	9.11	9.82
l-C_8N	0	0	8.6 ± 0.1	9.9 ± 0.2	8.58	9.81	8.30	9.80
[C_3]C_5N	0.71	0.33			-	9.67	-	9.69
[C_7]CN	1.27	0.60			8.49	9.48	8.21	9.65
l-C_9N	0	0	-	9.3 ± 0.1	9.10	8.92	9.23	9.17
[C_6]C_3N	1.65	0.69			9.26	9.78	8.96	10.05
[C_4]C_5N	1.72	1.13			8.86	-	8.59	-
l-$C_{10}N$	0	-	8.6 ± 0.1	9.9 ± 0.2	8.23	9.43	7.94	-
c-[$C_{10}N$]	1.51	-			7.79	8.06	-	-
l-$C_{11}N$	0	-	-	8.7 ± 0.2	8.69	8.53	8.83	8.92
c-[$C_{11}N$]	1.58				7.76	7.95	-	-
l-$C_{12}N$	0	-	8.4 ± 0.2	9.6 ± 0.3	7.96	9.01	7.63	-
c-[$C_{12}N$]	0.84	-			8.04	8.01	-	-

[a] All energies in eV.

[b] For C_4N-C_9N, the three lowest energy neutral isomers are listed, while for $C_{10}N$-$C_{12}N$, the linear and cyclic isomers are listed. See Figure 6 for isomer nomenclature.

[c] Singlet and triplet values denote IEs from the neutral doublet ground state to the cation singlet and triplet states.

[d] Geometry optimization and energy by ROHF/6-31G*.

[e] Geometry optimization and zero-point energy by ROHF/6-31G*.

Figure Captions

Figure 1: Schematic representation on the formation of C_nN clusters in the interstellar medium via photolysis of the closed shell precursors and bimolecular neutral-neutral reactions involving dicarbon molecules.

Figure 2: (a) Time-of-flight mass spectrum from the ablation of carbon rod with N_2O backing gas, recorded at 12.5 eV photon energy. The C_n, C_nO, and C_nN series are indicated. (b) Peak intensity vs. cluster size of C_nN^+ measured at photon energies of 11.5 eV (▲) and 12.5 eV (●).

Figure 3: PIE curves of C_nN (n=3-10), measured from 8.5 eV to 12.8 eV in 0.1 eV steps. Signal intensity normalized for comparison purpose.

Figure 4: PIE curves of even-carbon C_nN (n=4-12) from 8.0 eV to 11.4 eV in 0.05 eV steps. Main trace (●) is an average of 7 datasets with scan-to-scan variations shown in grey shading. The observed experimental ionization onsets are indicated by the black arrows (solid line for the first onset, dashed line for the second onset). For n=4-8, the calculated AIEs of the three lowest energy neutral isomers are shown on the PIE curves via the color coded lines. For n=10 and 12, the calculated AIEs for the linear and cyclic isomers are shown on the PIE curves. Red, blue, and green lines indicate CCSD(T) energies, while dark red and brown indicate B3LYP energies (solid and dashed lines denote ionization to the cation singlet and triplet states, respectively) .

Figure 5: PIE curves of odd-carbon C_nN (n=5-11) from 8.0 eV to 11.4 eV in 0.05 eV steps. Main trace (●) is an average of 7 datasets with scan-to-scan variations shown in grey shading. The observed experimental ionization onsets are indicated by the black arrows. For n=5-9, the calculated AIEs of the three lowest energy neutral isomers are shown on the PIE curves via the color coded lines. For n=11, the calculated AIEs for the linear and cyclic isomers are shown on the PIE curves. Red, blue, and green lines indicate CCSD(T) energies, while dark red and brown indicate B3LYP energies (solid and dashed lines denote ionization to the cation singlet and triplet states, respectively).

Figure 6: Optimized geometries of the low-lying (<2 eV) neutral isomers of C_8N. In parentheses are the relative energies, in eV, from the linear isomer (In black are CCSD(T) values and in gray are B3LYP values). The theoretical results for all the C_nN clusters studied in this paper are included in the supplementary information.

Figure 7: Optimized geometries of the linear isomers of C_nN clusters. Shown for each cluster size are the geometries of the neutral doublet ground state, the cation singlet state, and the cation triplet state. Detailed theoretical results on these isomers as well as other isomers are included in supplementary information.

Figure 8: Experimental and calculated AIEs to the cation singlet (a) and triplet (b) manifold of the linear isomer of C_nN. The cc-pVTZ basis set is used for both the B3LYP and the CCSD(T) calculations. All calculated AIEs include B3LYP/cc-pVTZ zero-point energy corrections.

Figure 1
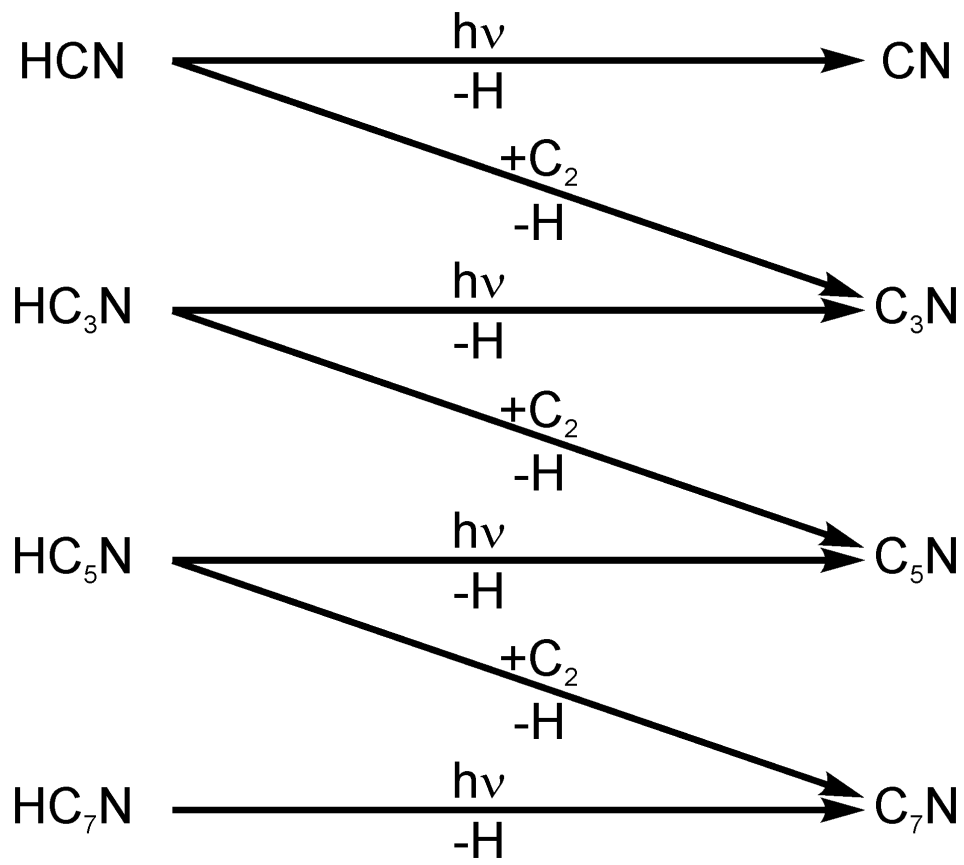
Figure 2
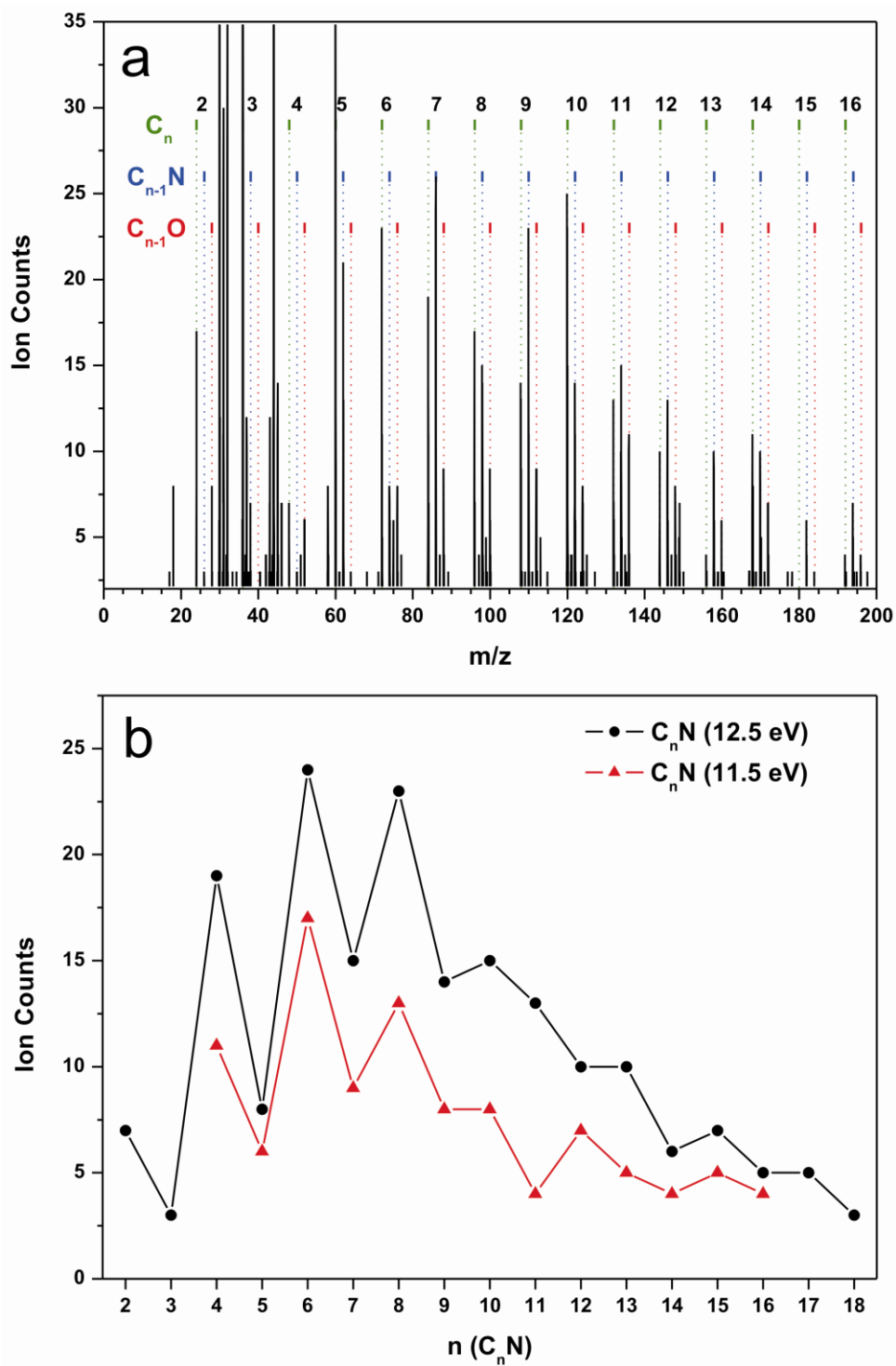
Figure 3
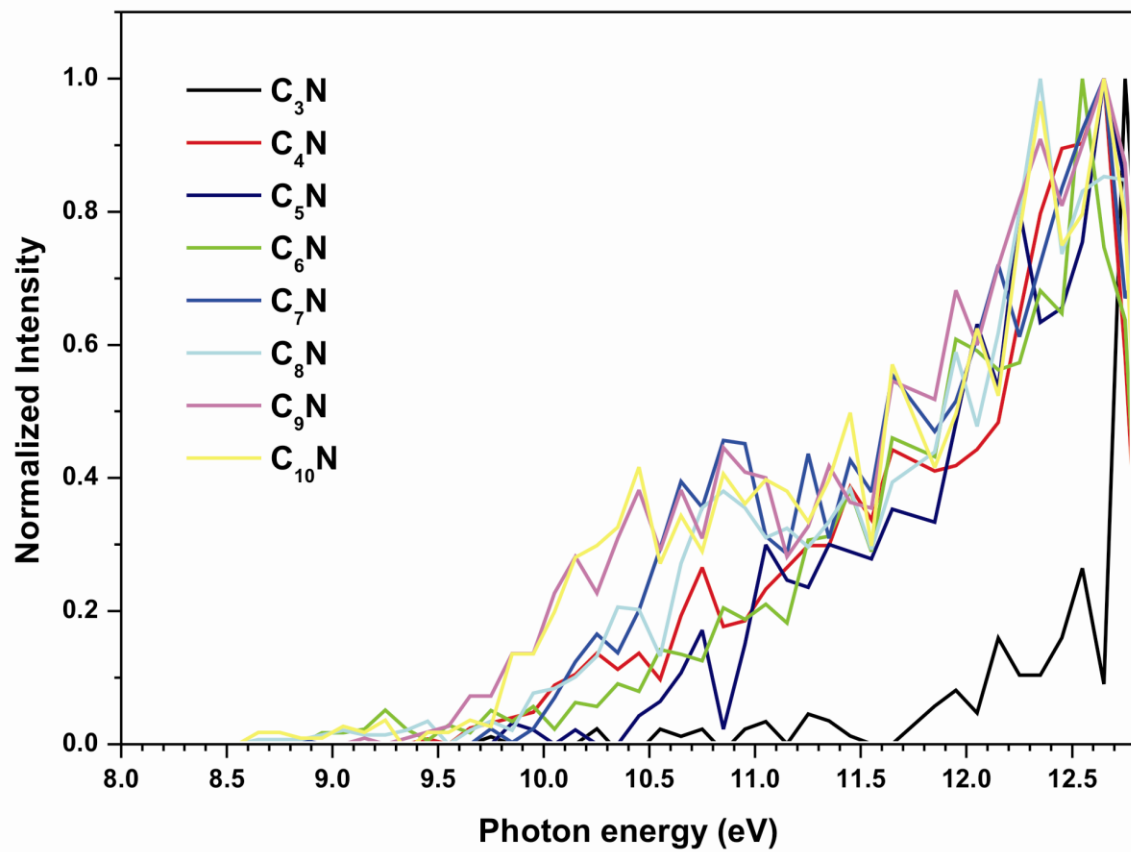
Figure 4
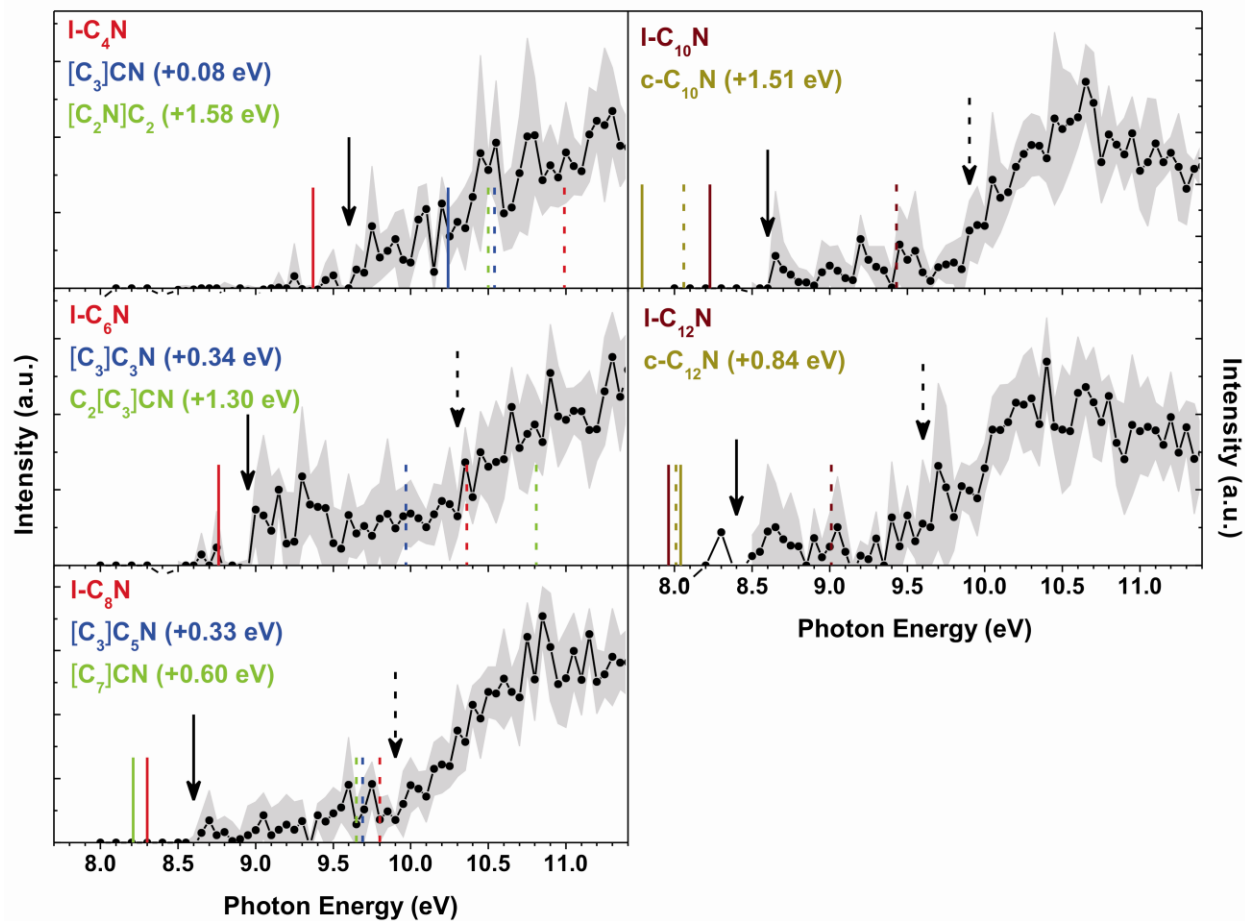
Figure 5
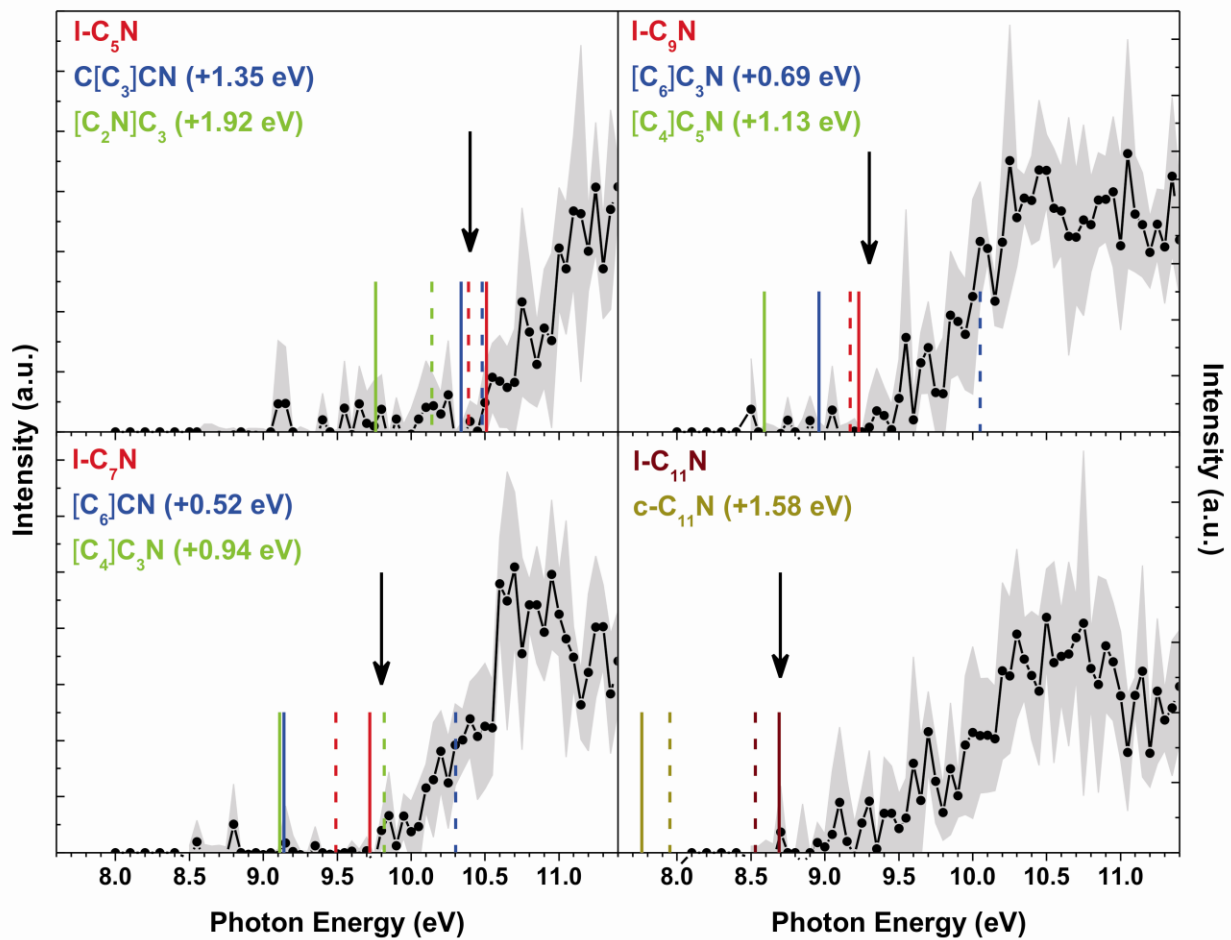
Figure 6

Figure 7

Figure 8